#### **ORIGINAL PAPER**



# Crimped fiber composites: mechanics of a finite-length crimped fiber embedded in a soft matrix

Nandan N. Pitre<sup>1</sup> · J. B. Moses<sup>2</sup> · Edith Tzeng<sup>2</sup> · Steven Abramowitch<sup>1</sup> · Sachin S. Velankar<sup>1,3,4,5</sup>

Received: 12 October 2022 / Accepted: 5 February 2023 © The Author(s), under exclusive licence to Springer-Verlag GmbH Germany, part of Springer Nature 2023

#### **Abstract**

Composites comprising crimped fibers of finite length embedded in a soft matrix have the potential to mimic the strain-hardening behavior of tissues containing fibrous collagen. Unlike continuous fiber composites, such chopped fiber composites would be flow-processable. Here, we study the fundamental mechanics of stress transfer between a single crimped fiber and the embedding matrix subjected to tensile strain. Finite element simulations show that fibers with large crimp amplitude and large relative modulus straighten significantly at small strain without bearing significant load. At large strain, they become taut and hence bear increasing load. Analogous to straight fiber composites, there is a region near the ends of each fiber which bears much lower stress than the midsection. We show that the stress-transfer mechanics can be captured by a shear lag model where the crimped fiber can be replaced with an equivalent straight fiber whose effective modulus is lower than that of the crimped fiber, but increases with applied strain. This allows estimating the modulus of a composite at low fiber fraction. The degree of strain hardening and the strain needed for strain hardening can be tuned by changing relative modulus of the fibers and the crimp geometry.

Keywords Collagen recruitment · Crimped fiber · Strain hardening · Fiber-reinforced composite

#### 1 Introduction

In a stress-free state, fibrous collagen in the body is organized with a periodic crimp pattern (Fratzl 2008; Kassab and Sacks 2016). This structure is observed in numerous tissues such as blood vessels, valve leaflets, intestine, ligaments, and tendons (Fratzl 2008; Gathercole and Keller 1991; Kassab and Sacks 2016). The crimped nature of collagen affects the mechanical and load-bearing properties of these tissues

- Sachin S. Velankar velankar@pitt.edu
   Department of Bioengineering, University of Pittsburgh,
- Department of Surgery, University of Pittsburgh, Pittsburgh, PA 15261, USA
- Department of Chemical Engineering, University of Pittsburgh, Pittsburgh, PA 15261, USA

Pittsburgh, PA 15261, USA

Published online: 02 March 2023

- Department of Mechanical Engineering and Materials Science, University of Pittsburgh, Pittsburgh, PA 15261, USA
- McGowan Institute of Regenerative Medicine, University of Pittsburgh, Pittsburgh, PA 15261, USA

(Diamant et al. 1972; Fratzl 2008; Fratzl et al. 1997; Kassab and Sacks 2016; Meyers et al., 2008; Rigby et al. 1959). The crimp pattern allows for highly nonlinear behavior wherein tissues act as soft materials at low strains as fibers uncrimp without bearing much load, but as stiffer materials at higher strains as fully uncrimped fibers become increasingly loadbearing (Canham et al. 1992; Diamant et al. 1972; Fratzl 2008; Fratzl et al. 1997; Gathercole & Keller 1991; Hilbert et al. 1996; Kassab & Sacks 2016Meyers et al., 2008). This phenomenon is well studied, and there have been numerous studies of collagen structure and its contribution to the mechanics of tissues (Canham et al. 1992; Hilbert et al. 1996; Maqueda et al. 2012; Muthukumar et al. 2018).

In computational studies, soft tissues are often modeled as composites comprising stiffer fibers embedded in a softer hyperelastic matrix, and their behavior has been modeled using finite element method for various types of fiber arrangements (Drach et al. 2016; Freutel et al. 2014; Gasser et al. 2006; Hiremath et al. 2018; Krishan 2019; López Jiménez & Pellegrino 2012; Politis 2014; Sun and Vaidya 1996). The fibers in these studies are treated as having periodic crimps defined by either helical (Freed and Doehring 2005) or planar sinusoid (Drach et al. 2016; Gasser et al.



2006; Krishan 2019) geometry. Boundary conditions are prescribed such that they undergo tensile loading within the simulations (Freutel, 2014; Politis 2014). Such computational studies have helped develop an understanding of the mechanisms responsible for the experimentally observed nonlinear elastic response of these tissues in response to externally applied loads (Hu et al. 2016; Karkan et al., 2019; Nezarati et al. 2015; Ravi et al. 2009; Wang et al. 2014; Zavan et al. 2021).

Devices intended for implantation within the body have sought to replicate the mechanical behavior of collagen-containing tissues, for example, using wavy knitted patterns as a graft material (Hu et al. 2016; Wang et al. 2014) to manufacture long continuous crimped fibers for applications such as vascular conduits (Hu et al. 2016; Jeffries et al. 2015; Karkan et al., 2019; Nezarati et al. 2015; Ravi et al. 2009; Wang et al. 2014; Zavan et al. 2021). Other approaches aiming to replicate these behaviors include electrospinning crimped fibers onto graft surfaces (Karkan et al., 2019; Nezarati et al. 2015; Zavan et al. 2021); using multilayer collagen fiber-reinforced tissue engineered composites (Ravi, 2009); suturable scaffolds (Chua et al. 2021; Jeffries et al. 2015), stents (Vearick et al. 2018), and bladder matrix(Stankus et al. 2008). However, a common limitation of these approaches is that it is difficult to process these materials into arbitrary shapes (Fidan et al. 2019; Zampaloni et al. 2007). Indeed, this problem is not unique to crimped fibers—all continuous fiber composites are difficult to fabricate into arbitrary shapes, though there has been more recent progress in this direction (Chang et al. 2022). Outside of the biomedical area, it has long been common to use chopped fiber composites (sometimes also called short fiber composites) to overcome the processability limitations of continuous fiber composites. Such composites are typically based on glass or carbon fibers cut to several-mm lengths and dispersed within a polymer matrix. Also, conceptually related are nanocomposites which comprise stiff nanoscale fillers of high aspect ratio such as carbon nanotubes, cellulose whiskers, or clay platelets dispersed into plastics (Chazeau et al. 2020; Loos & Manas-Zloczower 2013; Utracki 2010). Since the reinforcing fillers are no longer continuous, such chopped fiber composites or nanocomposites can be processed via conventional plastics processing operations including extrusion, molding, and extrusion-based 3D printing (De and White 1996; Komal et al. 2019; Krishan 2019; Ratner et al. 2004; Shao Yun Fu; Young 2015; Zhong et al. 2001). However, since the fillers are not in a crimped form, such composites do not replicate the strain-hardening behavior of collagen-containing tissues. The eventual goal of this research is to develop synthetic tissue substitutes where crimped fibers of a finite length act as reinforcing agents for a softer matrix. Such short fiber composites with crimped fibers may mimic the strain-hardening behavior of collagen-rich tissues. Their mechanical properties may be tuned by changing the properties of the fibers such as

the modulus, orientation, crimp geometry, and volume fraction of fibers (Curtin and Takeda 1998; Huang et al. 2021; Peel & Jensen 2001). Most importantly, similar to other chopped fiber composites, they would be processible, e.g., by molding or extrusion, thus facilitating manufacture of arbitrary shapes (Fu et al. 2009; Komal et al. 2019; Zhong et al. 2001).

This article is the first step in understanding the mechanics of short fiber-reinforced composites where we quantify the contribution of a single fiber to the properties of the composite. As reviewed in Sect. 2, such a single-fiber analysis has provided enormous insights into how a fiber's length and mechanical properties affect the modulus of the composite for non-crimped fibers. Thus, this study aims to take the same approach for crimped fiber composites by considering a single crimped fiber embedded in a sufficiently large soft matrix and examining the mechanics of uncrimping as the surrounding matrix is stretched.

This paper is organized as follows: Sect. 2 describes the shear lag theory for stress transfer in a straight fiber composite. A key result from the theory is that a certain length near the fiber ends bears much lower stress than the center of the fiber; accordingly, fibers that are too short are incompletely loaded. This low stress near the ends is expected to affect uncrimping behavior. Section 3 explains the simulation method. Section 4 presents the central results of the simulations including comparisons between crimped and straight fibers, and the effects of fiber geometry and modulus. Section 5 introduces the concept of an equivalent straight fiber which can approximate a crimped fiber, and therefore allows an estimate of the mechanical behavior of a composite containing a chopped crimped fiber. Section 6 concludes the paper with a brief summary.

# 2 Shear Lag Model for straight fiber composites

When a composite composed of straight fibers embedded in a softer matrix is placed under tensile stress, there occurs a transfer of stress from the matrix to the fiber thread (Hull and Clyne 1996). A commonly used model for this stress transfer is based on the shear lag theory (Cox 1952; Hull and Clyne 1996), first developed by Cox (1952) to model the behavior of discontinuous fiber composites when all of the fibers are aligned along the tensile direction. This theory assumes that each fiber (of length 2L and radius  $r_f$ ) is located at the center of a cylindrical matrix such that the ratio of fiber volume to the cylinder volume matches the volume fraction  $\phi$  of fibers in the composite. When the matrix is stretched along the x-direction (i.e., along the axis of the cylinder) to a strain of  $\varepsilon$ , the stress in the fiber rises from zero at the fiber ends as per



$$\sigma_f(x) = E_f \varepsilon \left[ 1 - \cosh\left(\frac{n}{r_f}x\right) . sech\left(n\frac{L}{r_f}\right) \right]$$
 (1)

where x is the coordinate along the fiber direction such that the fiber spans -L < x < L. Note that  $\sigma_f/E_f$  is simply the strain  $\varepsilon_f$  in the fiber. The quantity n is

$$n = \left[ \frac{2E_m}{E_f (1 + \nu_m) ln \left( \frac{1}{\phi} \right)} \right]^{\frac{1}{2}}$$
 (2)

where  $E_f$  and  $E_m$  are the moduli of the fiber and matrix, respectively, and  $v_m$  is the Poisson's ratio of the matrix. The quantity  $E_f/E_m$  will be called relative modulus henceforth. Exemplary profiles of  $\varepsilon_f(x) = \sigma_f/E_f$  are shown as solid lines in Fig. 2a discussed later. Integration of Eq. 1 over the fiber length gives the mean stress in the fiber as

$$\overline{\sigma_f} = E_f \varepsilon \left( 1 - \frac{\tanh(nL/r_f)}{nL/r_f} \right)$$
 (3)

Since the fibers are taken as aligned along the loading direction, the stress of the composite can be obtained by a weighted average of the fiber and the matrix. The ratio of this composite stress to the applied strain  $\varepsilon$  gives the composite modulus:

$$E_{com} = \frac{\overline{\sigma_f}}{\varepsilon} \phi + E_m (1 - \phi) \tag{4}$$

where the subscript com indicates composite.

It is also useful to define a dimensionless quantity  $\varepsilon_f(x) = \frac{\sigma_f(x)}{E_f}$  which is a measure of the strain in the fiber so that Eq. 1 can be rewritten as

$$\varepsilon_f(x) = \frac{\sigma_f(x)}{E_f} = \varepsilon \left[ 1 - \cosh\left(\frac{3x}{l_s}\right) . sech\left(\frac{3L}{l_s}\right) \right]$$
 (5)

where  $l_s = 3r_f/n$  is defined as the shear lag length. The factor of 3 is generally included in the definition of  $l_s$  because for sufficiently long fibers, the quantity in the square brackets is nearly 1 everywhere except within a distance of  $l_s$  from the ends.

Equations 1–5 offer key insights on how the length of fibers affects the mechanics of chopped fiber composites. Two limits can be identified readily. In the long fiber limit,  $\frac{L}{l_s} = \frac{nL}{3r_f} \gg 1$ , Eqs. 1 and 5 state that the entire length of the fiber except for the region within a distance  $l_s$  from the ends has  $\sigma_f(x) \approx E_f \varepsilon$ , or equivalently  $\varepsilon_f(x) \approx \varepsilon$ . Accordingly, most of the fiber is loaded to the highest extent possible at the applied strain, and hence Eq. 4 states that the composite modulus  $E_{com}$  is simply a volume-weighted average of the

moduli of the fiber and the matrix. However, the fiber strain drops to zero over the length of roughly  $l_s$  adjacent to each end. Within this region, stress is transferred by shear from the matrix to the fiber. In the short fiber limit, when  $\frac{L}{l_s} = \frac{nL}{3r_f}$  is on the order of 1 or smaller, Eq. 1 and 5 state that  $\sigma_f(x) < E_f \varepsilon$ , or  $\varepsilon_f(x) < \varepsilon$ . In this case, no portion of the fiber is fully loaded, and the chopped fiber is a relatively ineffective reinforcing agent.

Although the mechanics of crimped fiber composites are expected to differ from that of straight fiber composites, two effects may be expected from the discussion above. First, we anticipate that because the fiber can accommodate stretching by uncrimping, the actual strain in the fiber will be lower than the strain in the matrix, i.e., unlike Eq. 5,  $\varepsilon_f < \varepsilon$ is expected in the midsection of a fiber even if the fiber is very long. Under these uncrimping conditions, the midsection of the fiber contributes relatively little to the composite modulus because it bears only a low stress. Yet, as the fiber uncrimps, it will increasingly resemble a straight fiber, i.e.,  $\varepsilon_f$  will approach  $\varepsilon$  as the strain increases, leading to the strain hardening that mimics collagen-bearing tissues. Second, even for crimped fibers, we anticipate a near-end portion where the fiber experiences lower strain than the central portion. In this region, only partial uncrimping is expected, and hence this region will contribute less to strain hardening. The central goal of this article is to quantify these two effects as the crimp amplitude and the modulus of the fibers is varied.

With the above background, we can now formulate the questions to be addressed by simulations in this paper: (a) At what strain does the midsection of a long fiber uncrimp, how does the uncrimping affect the load borne by the fiber, and how does the uncrimping tune the strain-hardening behavior of the composite?, (b) Over what length near the fiber ends does the stress reduce significantly—which in turn defines the minimum length of crimped fiber necessary to achieve the desired strain hardening, and (c) How are the previous two questions affected by the fiber geometry and modulus of the fiber relative to the matrix?

### 3 Methods

We examined the mechanics of stress transfer of a crimped fiber embedded in a matrix using 3D finite element simulations. A single crimped fiber was embedded in a matrix of a relatively low Young's modulus and of dimensions  $2L_m$  along the x-direction,  $2H_m$  along the y-direction, and  $W_m$  along the z-direction (Fig. 1a). Taking advantage of symmetry, only half of the geometry was modeled. For straight fiber simulations, the fiber was specified as a hemicylinder of radius  $r_f$  and length  $2L=400r_f$  centered on the x-axis.



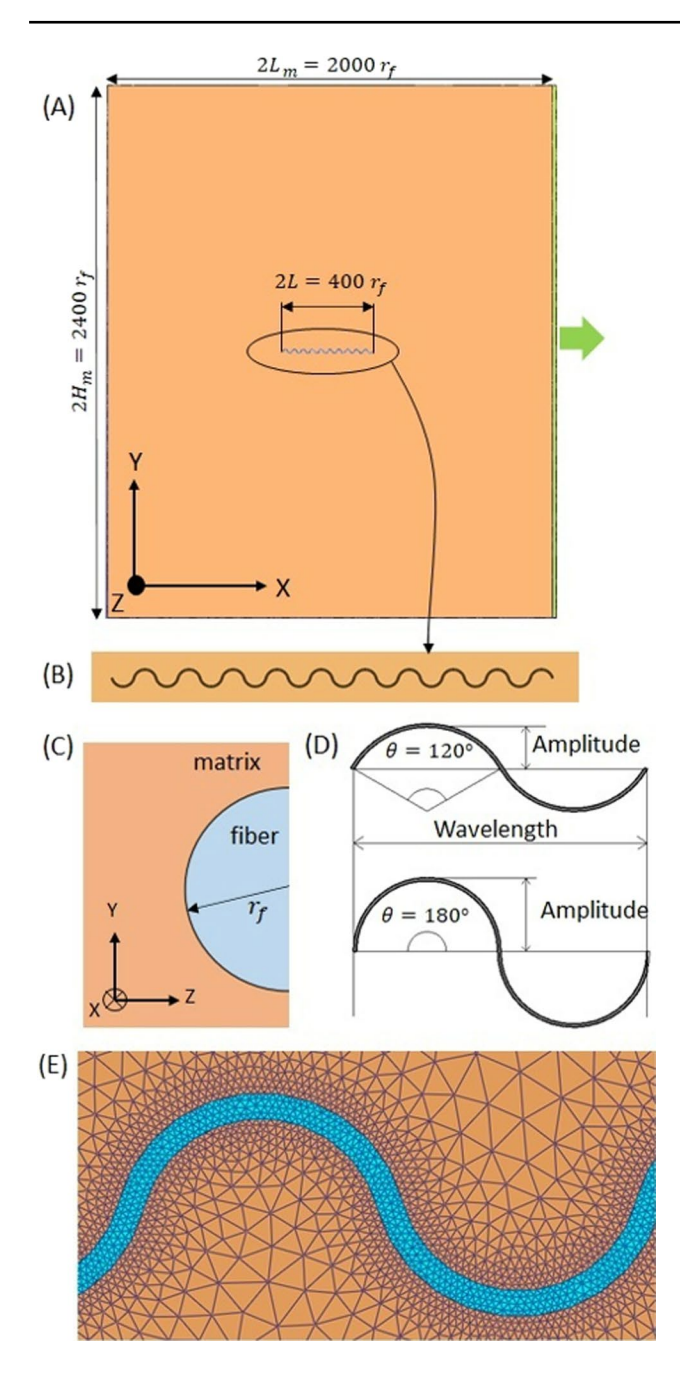
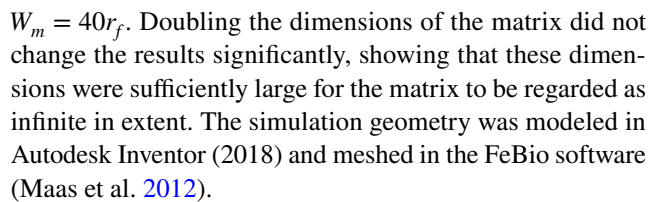


**Fig. 1** (**A**) Relative dimensions of the matrix and embedded fiber (**B**) magnified view of the geometry of the fiber, (**C**) semicircular cross section of the hemicylindrical fiber, (**D**) examples of how  $\theta$  affects the initial amplitude of the fiber, (**E**) tetrahedral adaptive mesh near the fiber-matrix interface illustrated for the fiber with  $\theta = 150^{\circ}$ 

The crimped fiber was modeled as a sequence of circular arcs, with the cross section being hemicylindrical (Fig. 1b-c). These arcs were defined by a parameter  $\theta$ , the projected angle. The wavelength of the crimps was fixed  $\lambda = 40r_f$  and thus a change in  $\theta$  corresponded to a change in the initial amplitude of the crimps (Fig. 1d). The dimensions of the matrix were chosen to be  $2L_m = 2000r_f$ ,  $2H_m = 2400r_f$  and



The left face of the matrix (the plane  $x = -L_m$ ) was held fixed while the right face  $(x = L_m)$  was displaced along the x-direction using a rigid body connection. The applied displacements corresponded to nominal strains (ratio of x-displacement to  $2L_m$ ) of up to 0.69. Symmetry boundary conditions were imposed on the center plane (z=0), whereas the remaining surfaces  $(y = \pm H_m \text{ and } z = W_m)$  were kept stress-free. Neo-Hookean material was chosen both for the fiber and the surrounding matrix. An adaptive tetrahedral mesh was used for the fiber and matrix. The mesh density was uniform across the fiber and the total number of elements increased with contour length of the fiber (i.e., with the amplitude), ranging from 21,916 for straight fiber to 31,620 for fiber with semicircular arcs. Facet-to-facet no-slip contact was applied between fiber and the matrix. Figure 1e shows a screenshot of the fiber mesh as seen at the central plane. The simulation results were found to be nearly identical when the mesh density was doubled, i.e., with eightfold increase in the number of elements, showing that the mesh density was adequate to correctly resolve the mechanics.

Two sets of simulations were conducted. In the first, the modulus ratio was held fixed at 1000 and four values of  $\theta$  (0°, 120°, 150° and 180°) were examined. The corresponding ratios of peak-to-trough amplitude to the wavelength were 0, 0.29, 0.38 and 0.5. This set of simulations allowed a clear assessment of the strain-dependent uncrimping of fibers, and the comparison with a straight fiber. In the second set, the initial amplitude was held fixed at  $\theta = 150^{\circ}$ , while the modulus ratio was varied. These simulations were also compared against simulations for a straight fiber geometry.

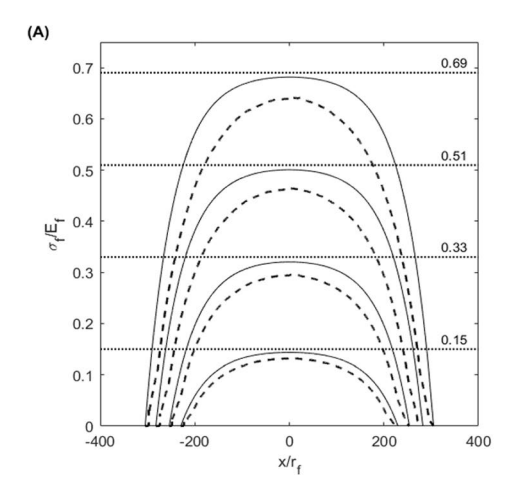
The simulations also provided end-reaction forces that had to be applied at the  $x = \pm L_m$  boundaries to maintain the specified displacement. These forces allowed calculation of the contribution of the embedded fiber to the stiffness of the composite as described in the Appendix.

#### 4 Results

# 4.1 Stress evolution of uncrimped versus crimped fiber

To illustrate the effect of crimps on the stretching behavior, Fig. 2 compares two cases:  $\theta = 0^{\circ}$ (straight fiber) vs  $\theta = 150^{\circ}$ , both at a relative modulus value of 1000. In both cases, we plot the stress profile in the fiber normalized by its modulus  $(\sigma_f/E_f)$  at four values of applied strain ( $\epsilon = 0.15, 0.33, 0.51$ 





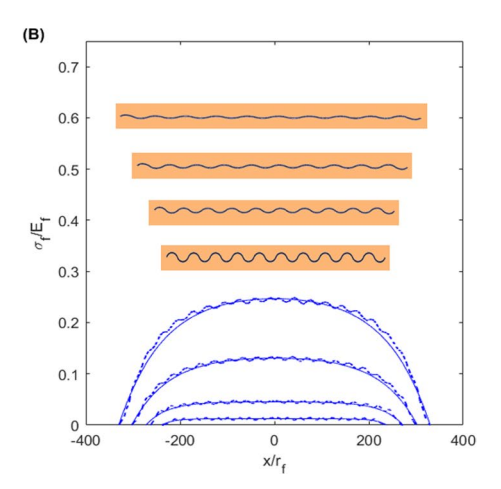


**Fig. 2** (**A**) Distribution of  $\varepsilon_f = \sigma_f/E_f$  for straight fiber: simulation data (black dashed line), Eq. 1 (black solid line), and (**B**):  $\sigma_f/E_f$ , where  $\sigma_f$  is the *x*-component of the Cauchy stress in the fiber; for crimped fiber with  $\theta=150^\circ$ : simulation data (blue dashed line), Eq. 6 (blue solid line, discussed in Sect. 5.1). In both graphs, the data are

shown at applied strain values (going from top to bottom) of 0.69, 0.51, 0.33, and 0.15. These four values are shown as horizontal dotted black lines in a. The images in b are screenshots of the fiber at the same four strains to illustrate uncrimping

and 0.69) which are indicated by the horizontal dotted lines in Fig. 2a. Here,  $\sigma_f$  refers to the  $\sigma_{xx}$  component of the in-fiber Cauchy stress tensor. Consistent with Sect. 2, the quantity of  $\sigma_f/E_f$  is defined as  $\varepsilon_f$  henceforth. Figure 2a shows that the profiles of  $\varepsilon_f$  in the straight fiber are in reasonable agreement with those predicted by the shear lag model Eq. 1 with no fitting parameters. The  $L/l_s$  calculated using Eq. 5 is 1.2, thus showing that the half-length of the fiber only slightly exceeds the shear lag length. Accordingly, Eq. 5 predicts, and simulations confirm, that the  $\varepsilon_f(x)$  in the midsection of the fiber is nearly constant and nearly equal to the applied strain, whereas it reduces to zero over a distance of roughly  $l_s$  from the ends.

Figure 2b shows the  $\varepsilon_f(x)$  profiles for an embedded crimped fiber with  $\theta=150^\circ$ . Although modulated by the crimp wavelength, the gross distribution of  $\varepsilon_f$  qualitatively resembles that in Fig. 2a: the midsection of the fiber has a nearly uniform value of  $\varepsilon_f$ , which reduces to zero near the ends. The major quantitative difference however is that the magnitude of  $\varepsilon_f$  near the middle is much lower than the applied strain because, as explained the end of Sect. 2, the applied strain is accommodated by uncrimping. A second, more subtle difference is that with increasing strain, the uniformly loaded midsection shrinks. Equivalently, there is an increase in the length near the ends where stress is lower than in the midsection. The solid lines in Fig. 2b are discussed later in Sect. 5.1, along with Eq. 6.

#### 4.2 Effect of initial amplitude

We will now quantify the uncrimping behavior by comparing fibers of various initial amplitudes (i.e., various  $\theta$ 

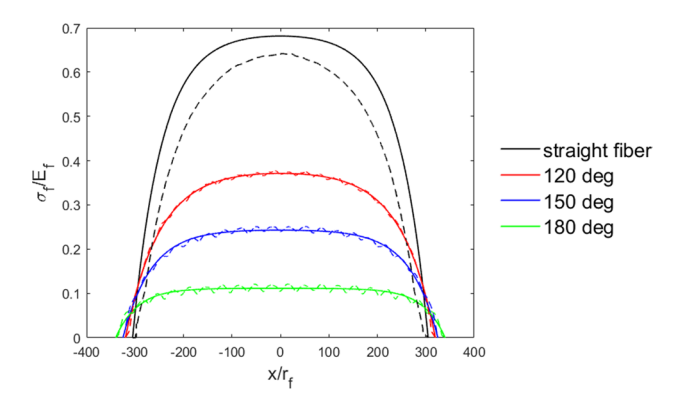


**Fig. 3** Distribution of  $\varepsilon_f(x) = \sigma_f(x)/E_f$  for different initial crimp amplitudes given by  $\theta=0^\circ$  (straight fiber), 120°, 150° and 180°; for  $E_f/E_m=1000$  and applied strain=69% (dashed lines), and Eq. 6 (solid lines, discussed in Sect. 5.1)

values), all at a relative modulus of 1000. Figure 3 shows the spatial distributions  $\varepsilon_f(x)$  of the various fibers, all at an applied stretch of 0.69. Snapshots of the fiber shape before and after stretching to an applied strain of 0.69 are shown in Fig. 4.

As in Fig. 2b, in all cases, the midsection of the fiber has an approximately flat distribution of  $\varepsilon_f$ . Further, the midsection also has a nearly uniform crimp amplitude (upper portion of Fig. 4). Both these observations suggest that the midsections of the fibers are isolated from any effects of shear lag from the fiber ends. Therefore, the mechanics of uncramping—independent of end-effects—can be quantified by examining a narrow section of the fiber near the middle. For this, we selected a two-wavelength-wide region at the center and calculated two quantities: the peak-to-trough



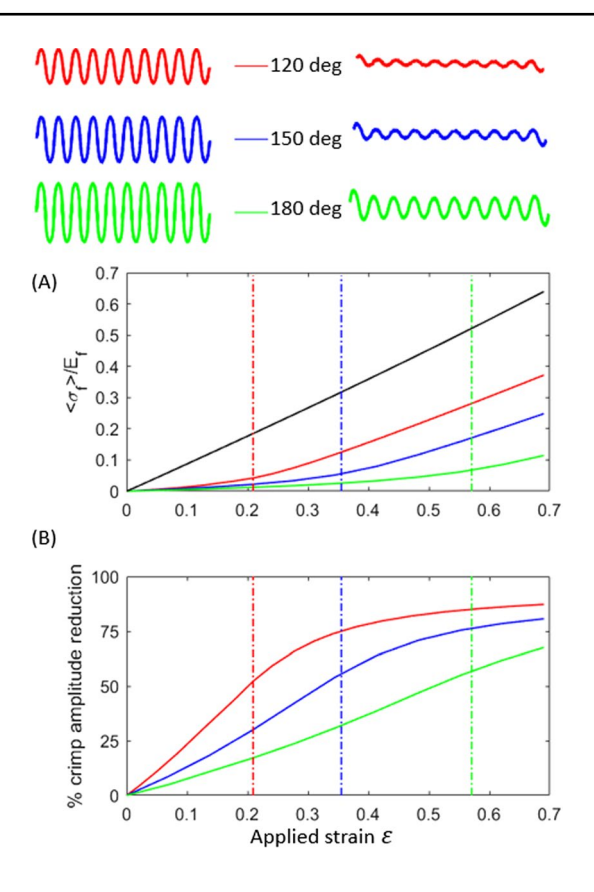


**Fig. 4** Upper images show amplitude profiles at applied strain  $\varepsilon = 0$  (top left) and  $\varepsilon = 0.69$  (top right). (**A**) Mean value  $\langle \varepsilon_f \rangle$  averaged over two wavelengths near the center, and (**B**) percent decrease in crimp amplitude in the midportion of the fiber for  $E_f = 1000$ . Vertical lines correspond to the strains needed for geometric straightening (see text)

amplitude which quantifies the geometric aspects of uncrimping, and the mean value of  $\langle \varepsilon_f \rangle = \langle \sigma_f \rangle / E_f$  which quantifies the strain borne by the fiber.

Figure 4a shows that for the straight fiber, the mean value of  $\langle \varepsilon_f \rangle$  is only slightly smaller than applied strain  $\varepsilon$ and increases almost linearly with  $\varepsilon$ . The slight nonlinearity is a geometric effect of the fiber length increasing as strain increases. For all the crimped fibers,  $\langle \varepsilon_{\rm f} \rangle < \varepsilon$  at small applied strain, and then grows nonlinearly in a manner similar to collagen recruitment. Concurrently, the amplitude reduces rapidly at low strain before leveling off as the fibers straighten. In effect, since the fiber straightens at small applied strain, further stretching must be accommodated by fiber stretching, rather than uncrimping. As discussed in Sect. 1, this increase in  $\langle \varepsilon_f \rangle$  (and hence  $\langle \sigma_f \rangle$ ) relates to strain hardening, and will be quantified later in this paper. As expected, all three quantities— $(\varepsilon - \langle \varepsilon_f \rangle)$ , the  $\varepsilon$  value at which  $\langle \varepsilon_f \rangle$  increases rapidly, and the  $\varepsilon$  value at which the amplitude significantly reduces—all increase with  $\theta$ . All three trends indicate an increasing degree of uncrimping with increasing initial crimp amplitude.

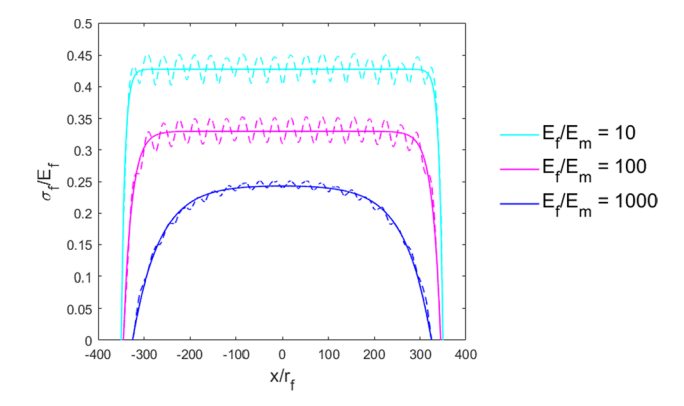


**Fig. 5** Distribution of  $\varepsilon_f(x) = \sigma_f(x)/E_f$  for  $E_f = 10$ , 100 and 1000, and  $\theta = 150^\circ$ 

The vertical lines in Fig. 4 correspond to "geometric straightening" and are calculated as the strain needed to make the end-to-end length of the uncrimped fibers equal to the contour length of the original crimped fiber. Figure 4b shows that at a strain corresponding to geometric straightening, the amplitude has only reduced by about 55–60% of the original value, i.e., a significant portion of the straightening continues beyond this point.

Finally, the amplitude profiles at the top of Fig. 4 show that the crimp amplitude does not decrease as much near the ends. This is not surprising: it is the tensile stress that induces straightening, and the end-region has a much lower tensile stress. Since the amplitude change is modest, one may expect that this end-region would make only a small contribution to strain hardening.

#### 4.3 Effect of relative modulus

The effect of relative modulus was examined by comparing fibers with three values of  $(E_f/E_m)=10$ , 100 and 1000. The angle was held fixed at  $\theta=150^\circ$ . Qualitatively, all three values of relative modulus show similar behavior, and in all cases, the midsection of the crimped fiber has a plateau in  $\varepsilon_f$ . Quantitatively, two effects are readily apparent. First, with decreasing relative modulus, the  $\varepsilon_f$  increases (Fig. 5) indicating that fibers of lower stiffness accommodate the applied strain by stretching rather than uncrimping. Second, as fiber modulus reduces, the midsection where the fiber has nearly constant  $\varepsilon_f$  becomes wider (equivalently, the near-end region of the fiber which bears a lower stress becomes narrower).

Analogous to Fig. 4, Fig. 6a shows the evolution of the average value  $\langle \varepsilon_f \rangle$  over two wavelengths at the center of the fiber, whereas Fig. 6b shows the % decrease in crimp amplitude in the midsection. The crimp amplitude decreases much less with decreasing relative modulus: for a relative modulus of 1000, the amplitude reduces by 82% of the original value, whereas for a relative modulus of 10, the decrease is



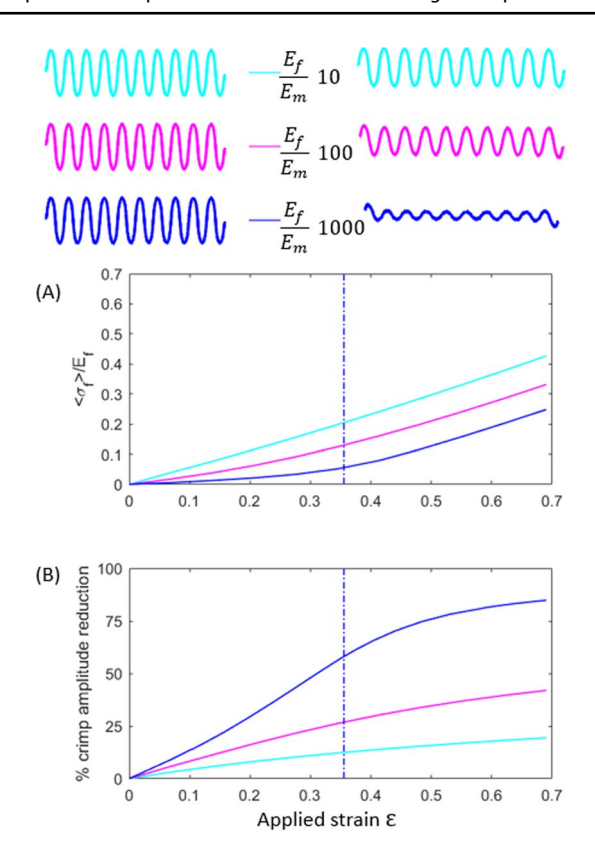


**Fig. 6** Upper images show amplitude profiles at applied strain  $\varepsilon = 0$  (top left) and  $\varepsilon = 0.69$  (top right). Note that the end-to-end length for profiles on the right are 69% longer than those on the left. (A) Mean value  $\langle \varepsilon_f \rangle$  averaged over two wavelengths near the center, and (B) percent decrease in crimp amplitude in the midsection of the fiber for  $\theta = 150^\circ$ 

only 21%. Similar to Fig. 4, beyond the strain for geometric straightening (vertical line), the decrease in amplitude with strain continues, but becomes more gradual (Fig. 6b).

### 5 Discussion

The simulations show that at any given value of applied strain, the midsection of the crimped fiber bears a lower stress than a straight fiber of the same aspect ratio and modulus. Further, similar to a straight fiber, the crimped fiber has a near-end region that is loaded less than the midsection. The ultimate goal of these simulations is to inform the design of composites that use chopped crimped fibers to achieve strain-hardening behavior that mimics collagen-rich tissues. In this Discussion section, we do so in two steps: Sect. 5.1 proposes that the crimped fiber may be treated as an equivalent straight fiber. Section 5.2 then uses the equivalent straight fiber concept to estimate the modulus of composites comprising crimped fibers embedded in a soft matrix.

# 5.1 Equivalent straight fiber model

As discussed above, Figs. 2, 3 and 5 show that the gross shape of  $\varepsilon_f(x)$  profile resembles that of straight fibers, albeit with a wavelength-scale modulation. This suggests that we may regard the crimped fiber as an equivalent straight fiber which has the same end-to-end length as the crimped fiber, but a different effective radius, shear lag length, and stiffness. Accordingly, the stress in the crimped fiber may be postulated to follow Eq. 1, but in modified form

$$\sigma_{f}(x) = E_{f}^{eff} \varepsilon \left[ 1 - cosh \left( \frac{n^{eff}}{r_{f}^{eff}} x \right) . sech \left( n^{eff} \frac{L}{r_{f}^{eff}} \right) \right]$$
 (6)

where  $n^{eff}$  is defined identically as Eq. 2, but with  $E_f$  replaced with  $E_f^{eff}$ . Here,  $E_f^{eff} < E_f$  is the modulus of the equivalent straight fiber. For a sufficiently long crimped fiber, Eq. 6 has a flat profile near its middle, however, unlike for a straight fiber, the magnitude of the stress far from the ends is  $E_f^{\it eff} \, \epsilon$ . The ratio  $E_f^{\it eff}/E_f$  may be regarded as a fiber efficiency factor, and we anticipate that its value increases with applied strain as the fiber uncrimps and approaches a straight fiber. Further, the stress decays toward zero within an effective shear lag distance  $I_s^{eff} = 3r_f^{eff}/n^{eff}$ . Equation 6 is fitted to the strain profiles using  $E_f^{eff}$  and  $r_f^{eff}$  as the fitting parameters, and the solid lines in Figs. 2b, 3, and 5 show that reasonable fits are obtained. The corresponding fitting parameters, and the calculated values of  $l_s^{eff}$ , all suitably non-dimensionalized, are shown in Fig. 7a-c at fixed modulus ratio, and e-g for fixed amplitude. The shear lag length for the fiber with large amplitude ( $\theta = 180$ ) and modulus ratio of 1000 is smaller than half of the crimp wavelength for  $\varepsilon < 0.15$ , making the fits unreliable for small strains for this fiber, and hence are not reported in Fig. 7.

The results of Fig. 7 can now guide the design of composites based on chopped crimped fibers. Figure 7a, e quantifies the degree to which sufficiently long crimped fibers can act as strain-hardening reinforcers. Specifically, Fig. 7a shows that at a relative modulus of 1000, crimped fibers have  $E_f^{eff}/E_f < 0.1$  at small strain, i.e., they have an effective modulus that is over tenfold lower than their actual modulus. Equivalently, the stress in the fiber is less than 10% of the value expected for a long straight fiber. With increasing strain, their effective modulus increases analogous to collagen recruitment, and further, fibers with larger initial crimp amplitudes require larger strains to be recruited. Indeed, at the highest amplitude corresponding to  $\theta = 180^{\circ}$ ,  $E_f^{eff}/E_f$  remains below 0.1 up to an applied strain of nearly 0.52, indicating that the fibers are approximately inextensible, i.e., they uncrimp with very little stretching. An unexpected result from Fig. 7e is that for fibers with a modulus



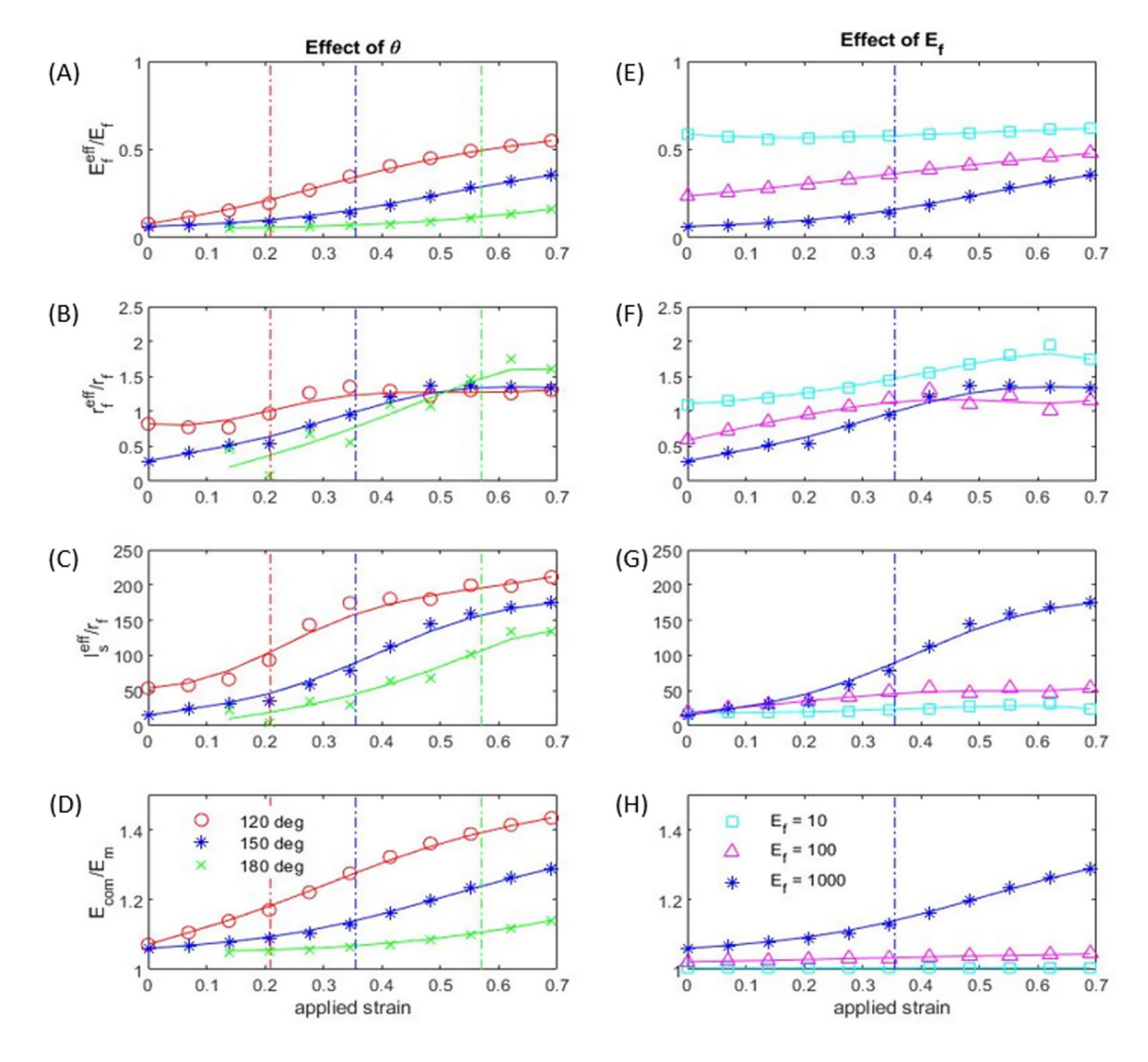


**Fig. 7** Variation in (A&E) equivalent effective modulus factor  $E_f^{eff}/E_f$ ), (B&F) normalized effective radius  $(r_f^{eff}/r_f)$ , (C&G) normalized effective shear lag length  $(f_s^{eff}/r_f)$  and (D&H) normalized modulus of the composite  $(E_{com}/E_m)$  with applied strain using  $\phi=1\times 10^{-3}$ . Left column shows effect of varying crimp amplitude

at fixed relative modulus of 1000. Right column shows effect of relative modulus at fixed crimp amplitude corresponding to  $\theta=150^\circ$ . Vertical lines indicate the strains for geometric straightening of the crimps

ratio of 10,  $E_f^{\it eff}$  is nearly independent of  $\varepsilon$  suggesting that these fibers are altogether ineffective at realizing strain hardening, i.e., crimped fibers with the geometry used here can only confer significant strain hardening if their modulus is at least 100-fold larger than of the matrix.

Figure 7a, e only comments on the uncrimping behavior of sufficiently long fibers since the value of  $E_f^{\rm eff}$  only determines stress in the fiber far from the ends. To understand fiber length effects, we turn to Fig. 7c, g which plots the strain-evolution of the effective shear lag length  $I_s^{\rm eff}$ . As discussed above, a straight fiber with  $L < l_s$  cannot be loaded to its fullest extent and hence may be regarded as an

ineffective reinforcing agent. Analogously, for a crimped fiber if  $L < l_s^{eff}$ , the midsection of the fiber bears a stress even lower than  $E_f^{eff} \varepsilon$ . Such a fiber will uncrimp less than a long fiber, and be unsuitable to realize strain-hardening behavior. Figure 7c shows that for a relative modulus of 1000,  $l_s^{eff}$  is comparable to the wavelength at small strain, but increases significantly with strain, i.e., a fiber that is long enough to approximate infinite-length at small strain may have more significant end-effects at large strain.



#### 5.2 Modulus of composites

The modulus of such composites can be estimated from adding the matrix and the fiber contributions as per Eq. 4. We now take advantage of the equivalent fiber concept and hence integrate Eq. 6 over the fiber length to estimate the mean stress in the fiber,  $\tilde{\sigma}_f$ . The final expression for  $\tilde{\sigma}_f$  is identical to Eq. 3, but with effective quantities on the right hand side. Appendix A shows that an independent method of estimating  $\overline{\sigma_f}$  using end-reaction forces is in excellent agreement with the equivalent fiber approach. The values of  $E_{com}$  thus calculated from Eq. 4 are plotted in Fig. 7d, h. They show how the desired level of strain hardening can be achieved by an appropriate choice of initial amplitude and relative modulus of the fibers. For small strains, all the composites (but especially those with crimped fibers of high initial amplitude) have a modulus that is only slightly higher than of the matrix. At high relative modulus, the fibers make increasing contributions to modulus as strain increases, analogous to collagen recruitment. The strain for onset of strain hardening approximately matches the geometric limit of the strain needed to completely uncrimp the fibers. As mentioned above, the degree of strain hardening is very modest for modulus ratios of 100 and 10 (Fig. 7h), i.e., for the geometry considered here, crimped fibers would be useful for strain hardening only if the relative modulus is on the order of 1000 or higher.

The limitations of Eq. 4 must be noted: it is only justifiable if the fibers are aligned along the tensile direction and dilute (and hence their stress fields are non-interacting). In our calculations, we have used a volume fraction ( $\phi$ ) of  $1 \times 10^{-3}$  for the fiber in the simulated matrix as representative of dilute conditions. A more detailed computational study would be needed to identify the volume fraction at which fibers interact with each other, and to estimate the modulus of the crimped fiber composites with a high volume fraction of fibers.

# 6 Summary and Conclusions

The crimped structure of collagen fibers is well-recognized as contributing to the strain-hardening behavior of tissues. We consider the mechanics of composites composed of chopped crimped fibers embedded in a softer matrix. Such discontinuous fiber composites have the potential to show strain-hardening behavior while also being flow-processible. This paper examines the behavior of a single crimped fiber of a specified length as the matrix embedding the fiber is stretched. Simulations show that such a crimped fiber bears lower load than a straight fiber of the same modulus, but that the load borne by the fiber increases nonlinearly as the matrix strain increases. Concurrently, the fiber is found to

straighten (i.e., the crimp amplitude reduces) analogous to collagen recruitment.

As with traditional chopped fiber (also known as short fiber) composites, there are significant end-effects. There is a certain length near the ends of the crimped fiber where the stress is significantly lower than the stress in its midsection, analogous to the shear lag length in straight fiber composites. Thus, crimped fibers can significantly contribute to the modulus of the composite (and hence to the strain-hardening behavior of the composite) only if the fiber is much longer than this shear lag length.

Broadly, the stress profiles in crimped fibers resemble those in straight fiber composites, and hence we develop the concept of an equivalent fiber. Accordingly, a crimped fiber can be treated as an equivalent straight fiber, but with an effective modulus and effective radius that is different from its true modulus and radius. This allows prediction of the contribution of the fiber to the modulus of the composite.

We quantify how all the relevant quantities: the load-bearing capability of the fiber, the shear lag length, and the modulus of the composite, depend on the crimp amplitude and the modulus of the fiber relative to the matrix. Fibers with small crimp amplitude or modest relative modulus are load-bearing even at small strain. Such fibers raise the modulus of the composite, but not in a strain-hardening fashion. In contrast, fibers with large crimp amplitude and large relative modulus first straighten significantly without bearing significant load, and then bear increasing load once they become taut. This mimics the strain-hardening behavior of collagencontaining tissues such as skin or arterial walls. Surprisingly high relative modulus values, on the order of 1000, are necessary to see significant strain-hardening behavior. In summary, the degree of nonlinearity and the extent of

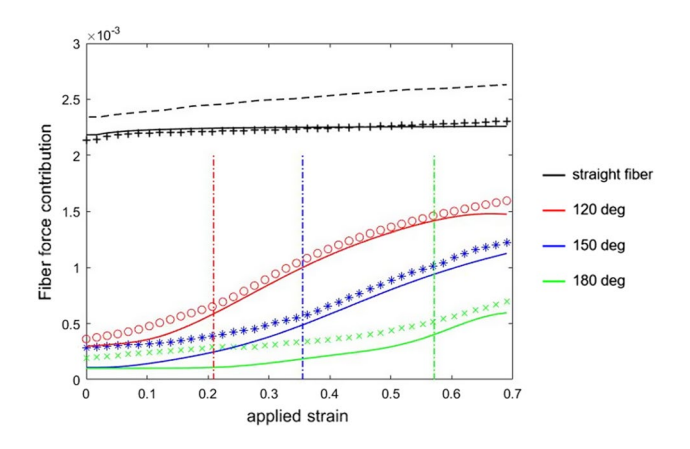


**Fig. 8** Comparison of two different methods of calculating the contribution of single fibers to the force in the composite. Stars show the value of  $\beta$  calculated from the end-reaction forces (Eq. A1). Solid lines are calculations of  $\alpha$  from the equivalent fiber model (Eq. A2). Dashed black line is the prediction of shear lag model (Eq. A3) with no fitting parameters



fiber loading can be controlled by changing fiber parameters such as fiber length, relative stiffness, and crimp geometry.

**Appendix** 

As illustrated in Fig. 1 in the main text, the simulation outputs the tensile force F that must be applied on the boundary at  $x = L_m$  to achieve the desired strain. Simulations were also conducted without a fiber to obtain the force  $F_m$  when the matrix alone is stretched. We may now define  $\beta$  as

$$\beta = \frac{F - F_m}{F_m} \tag{A1}$$

 $\beta$  represents the fractional extra force needed to stretch the matrix due to the presence of the fiber.

The quantity  $\beta$  may be compared against the force-contribution of the fiber calculated using the effective fiber approach described in the main text. The quantity  $\frac{\overline{\sigma_f}}{E_n \epsilon}$  defined in Sect. 2, as the ratio of average stress in the fiber to that in the matrix, is obtained from simulation data. The contribution of the single fiber is then estimated by integrating the stress profile over the entire fiber to obtain

$$\alpha = \frac{\overline{\sigma_f}}{E_m \varepsilon} . \phi = \frac{E_f^{eff}}{E_m} \left( 1 - \frac{\tanh\left(n^{eff} L/r_f^{eff}\right)}{n^{eff} L/r_f^{eff}} \right) \phi \tag{A2}$$

where  $\phi$  is the volume fraction of the fiber in the matrix.  $\alpha$  represents the ratio of average stress in fiber to average stress in the matrix, when experiencing the same strain, scaled to the volume fraction of the thread.

The contribution of the fiber to the composite stiffness obtained in these two distinct ways— $\beta$  using the total force, and  $\alpha$  using the average of the stress distribution—are compared in Fig. 8 for the same simulations as Figs. 3 and 4. Figure 8 also includes a theoretical value of  $\alpha$  for a straight fiber from the shear lag model (dashed). This is obtained from averaging Eq. 3 in the main text over the length of the straight fiber

$$\alpha^{straight} = \frac{E_f}{E_m} \left( 1 - \frac{tanh(nL/r)}{nL/r} \right) \phi \tag{A3}$$

For the straight fiber,  $\alpha$  and  $\beta$  start at a higher value and remain nearly constant. The slight increase in the quantities is due to increase in the fiber length as strain increases. For the crimped fibers,  $\alpha$  and  $\beta$ , start at low values and increase nonlinearly with strain, indicating increasing contribution as the fiber uncrimps. The good agreement between the two methods establishes that Eq. A2 can be used to accurately

obtain the contribution of the crimped fiber to the composite once the quantities  $E_f^{\it eff}$  and  $r_f^{\it eff}$  are found for the equivalent fibers

Author Contributions All authors contributed to the research presented. Conceptualization was contributed by NP, SV, and JBM; methodology was contributed by NP and SA; formal analysis was contributed by NP; writing—original draft preparation was contributed by NP; writing—reviewing and editing was contributed by NP, ET, SV, and SA; funding acquisition was contributed by ET and SV.

Funding NP, ET, and SV acknowledge support from NSF-1824708 and NIH R56-HL142743-01. SV acknowledges support from NSF-1561789 and NSF-2036164. SA acknowledges support from NSF-2053851. JBM acknowledges support from NHLBI T32 HL098036-12. NP is grateful to the Berenfield Fellowship from the University of Pittsburgh. The University of Pittsburgh holds a Physician-Scientist Institutional Award from the Burroughs Welcome Fund—JBM.

Availability of data and materials Not applicable.

#### **Declarations**

Ethical approval Not applicable.

**Competing interests** The authors declare that they have no competing interests in this research.

# References

Canham PB, Whittaker P, Barwick SE, Schwab ME (1992) Effect of pressure on circumferential order of adventitial collagen in human brain arteries. Can J Physiol Pharmacol 70(2):296–305. https:// doi.org/10.1139/y92-037

Chang H, Liu Q, Zimmerman JF, Lee KY, Jin Q, Peters MM, Rosnach M, Choi S, Kim SL, Ardoña HAM, Macqueen LA, Chantre CO, Motta SE, Cordoves EM, Parker KK (2022) Recreating the heart 's helical structure-function relationship with focused rotary jet spinning. Science 377(6602):180–185

Chazeau L, Gauthier C, Vigier G, Cavaillé J, Chazeau L, Gauthier C, Vigier G, Relationships JC (2020) Relationships between microstructural aspects and mechanical properties in polymer based nanocomposites To cite this version: HAL Id: hal-02917761 Please cite as: Relationships between microstructural aspects and mechanical properties in polymer based.

Chua CYX, Liu HC, Di Trani N, Susnjar A, Ho J, Scorrano G, Rhudy J, Sizovs A, Lolli G, Hernandez N, Nucci MC, Cicalo R, Ferrari M, Grattoni A (2021) Carbon fiber reinforced polymers for implantable medical devices. Biomaterials. https://doi.org/10.1016/j.biomaterials.2021.120719

Cox HL (1952) The elasticity and strength of paper and other fibrous materials. Br J Appl Phys 3(3):72–79. https://doi.org/10.1088/0508-3443/3/3/302

Curtin WA, Takeda N. (1998). Tensile strength of fiber reinforced composites: application to polymer matrix composites. *Composite Materials*, 32.

De SK, White JR (1996) Short fibre-polymer composites. Woodhead Publishing, Sawston

Diamant J, Keller A, Baer E, Litt M, Arridge RG (1972) Collagen; ultrastructure and its relation to mechanical properties as a



- function of ageing. Proc R Soc Lond Ser B. Biol Sci, 180(60): 293–315. https://doi.org/10.1098/rspb.1972.0019
- Drach B, Kuksenko D, Sevostianov I (2016) Effect of a curved fiber on the overall material stiffness. Int J Solids Struct 100–101:211–222. https://doi.org/10.1016/j.ijsolstr.2016.08.018
- Fidan I, Imeri A, Gupta A, Hasanov S, Nasirov A, Elliott A, Alifui-Segbaya F, Nanami N (2019) The trends and challenges of fiber reinforced additive manufacturing. Int J Adv Manuf Technol 102(5–8):1801–1818. https://doi.org/10.1007/s00170-018-03269-7
- Fratzl P, Misof K, Zizak I, Rapp G, Amenitsch H, Bernstorff S (1997) Fibrillar structure and mechanical properties of collagen. J Struct Biol 122:119–122
- Fratzl P (2008) Collagen: structure and mechanics, an introduction, pp. 1–13. https://doi.org/10.1007/978-0-387-73906-9\_1
- Freed AD, Doehring TC (2005) Elastic model for crimped collagen fibrils.

  J Biomech Eng 127(4):587–593. https://doi.org/10.1115/1.1934145
- Freutel M, Schmidt H, Dürselen L, Ignatius A, Galbusera F (2014) Finite element modeling of soft tissues: material models, tissue interaction and challenges. Clin Biomech 29:363–372. https://doi. org/10.1016/j.clinbiomech.2014.01.006
- Fu S, Lauke B, Mai YW (2009) Science and engineering of short fibre reinforced polymer composites. Elsevier Science, Amsterdam
- Gasser TC, Ogden RW, Holzapfel GA (2006) Hyperelastic modelling of arterial layers with distributed collagen fibre orientations. J R Soc Interface 3:15–35. https://doi.org/10.1098/rsif.2005.0073
- Gathercole LJ, Keller A (1991) Crimp morphology in the fibre-forming collagens. Matrix 11(3):214–234. https://doi.org/10.1016/S0934-8832(11)80161-7
- Hilbert SL, Sword LC, Batchelder KF, Barrick MK, Ferrans VJ (1996) Simultaneous assessment of bioprosthetic heart valve biomechanical properties and collagen crimp length. J Biomed Mater Res 31(4):503–509. https://doi.org/10.1002/(SICI)1097-4636(199608) 31:4%3c503::AID-JBM10%3e3.0.CO;2-H
- Hiremath CP, Senthilnathan K, Naik NK, Guha A, Tewari A (2018) Numerical study and experimental validation of effect of varying fiber crack density on stiffness reduction in CFRP composites. J Mater Eng Perform 27(4):1685–1693. https://doi.org/10.1007/ s11665-018-3275-0
- Hu JJ, Lu PC, Lou CW, Lee MC, Lin JH (2016) Small-diameter vascular grafts composed of polyester/spandex fibers: manufacturing techniques and property evaluations. Mater Lett 171:42–45. https://doi.org/10.1016/j.matlet.2016.01.154
- Huang ZM, Guo WJ, Huang HB, Zhang CC (2021) Tensile strength prediction of short fiber reinforced composites. Materials. https:// doi.org/10.3390/ma14112708
- Hull DC, Clyne TW (1996) Introduction to composite materials, 2nd edn. Cambridge University Press, Cambridge
- Jeffries EM, Allen RA, Gao J, Pesce M, Wang Y (2015) Highly elastic and suturable electrospun poly(glycerol sebacate) fibrous scaffolds. Acta Biomater 18:30–39. https://doi.org/10.1016/j.actbio. 2015.02.005
- Kassab GS, Sacks MS (2016) Structure-based mechanics of tissues and organs.https://doi.org/10.1007/978-1-4899-7630-7
- Komal UK, Lila MK, Chaitanya S, Singh I (2019) Fabrication of short fiber reinforced polymer composites. In P. K. Bajpai, (Ed.), Reinforced polymer composites: processing, characterization and post life assessment. Wiley, Berlin. https://doi.org/10.1002/97835 27820979.ch2
- Krishan KC (2019) Composite materials: science and engineering. Springer, Berlin
- Loos MR, Manas-Zloczower I (2013) Micromechanical models for carbon nanotube and cellulose nanowhisker reinforced composites. Polym Eng Sci 53(4):882–887. https://doi.org/10.1002/pen.23313

- López Jiménez F, Pellegrino S (2012) Constitutive modeling of fiber composites with a soft hyperelastic matrix. Int J Solids Struct 49(3–4):635–647. https://doi.org/10.1016/j.ijsolstr.2011.11.006
- Maas SA, Benjamin E, Ateshian GA, Weiss JA (2012) FEBio: Finite elements for biomechanics. J Biomech Eng 134(1):011005
- Maqueda, I., Pellegrino, S., & Mejia-Ariza, J. M. (2012). Characterization of a high strain composite material. Collection of technical papers—AIAA/ASME/ASCE/AHS/ASC structures, structural dynamics and materials conference, pp 1–12. https://doi.org/10.2514/6.2012-1909
- Muthukumar M, Prasath J, Desai YM, Naik NK (2018) Mechanical behavior of unidirectional composites with hexagonal and uneven distribution of fibers in the transverse cross-section. J Compos Mater 52(22):2985–3000. https://doi.org/10.1177/0021998318 759742
- Nezarati RM, Eifert MB, Dempsey DK, Cosgriff-Hernandez E (2015) Electrospun vascular grafts with improved compliance matching to native vessels. J Biomed Mater Res—Part B Appl Biomater 103(2):313–323. https://doi.org/10.1002/jbm.b.33201
- Peel LD, Jensen DW (2001) Response of fiber-reinforced elastomers under simple tension. J Compos Mater 35(2):96–137. https://doi. org/10.1106/V3YU-JR4G-MKJG-3VMF
- Politis D (2014) Finite element analysis of Tendon's collagen network in three dimensions
- Ratner B, Hoffman AS, Shoen FJ, Lemons JE (2004) Biomaterials Science an introduction to materials in medicine, 2nd edn. Elsevier Academic Press, Cambridge
- Ravi S, Qu Z, Chaikof EL (2009) Polymeric materials for tissue engineering of arterial substitutes. Vascular. https://doi.org/10.2310/6670.2008.00084
- Rigby BJ, Harai N, Spikes JD, Eyring H (1959) The mechanical properties of rat tail tendon. J Gen Physiol, 43, 265–283. https://rupress.org/jgp/article-pdf/43/2/265/1242194/265.pdf
- Shao Yun Fu, Bl. Science and engineering of short fi bre reinforced polymer composites Related titles.
- Stankus JJ, Freytes DO, Badylak SF, Wagner WR (2008) Hybrid nanofibrous scaffolds from electrospinning of a synthetic biodegradable elastomer and urinary bladder matrix. J Biomater Sci Polym Ed 19(5):635–652. https://doi.org/10.1163/1568562087 84089599
- Sun CT, Vaidya RS (1996) Prediction of composite properties from a representative volume element. Compos Sci Technol. https://doi. org/10.1016/0266-3538(95)00141-7
- Utracki LA (2010) Clay-containing polymeric nanocomposites and their properties. IEEE Electr Insul Mag 26(4):8–17. https://doi.org/10.1109/MEI.2010.5511184
- Vearick SB, Demétrio KB, Xavier RG, Moreschi AH, Muller AF, Sanches PRS, dos Santos LAL (2018) Fiber-reinforced silicone for tracheobronchial stents: an experimental study. J Mech Behav Biomed Mater 77:494–500. https://doi.org/10.1016/j.jmbbm. 2017.10.013
- Wang FJ, Mohammed A, Li CJ, Wang L (2014) Promising poly(ε -caprolactone) composite reinforced with weft-knitted polyester for small-diameter vascular graft application. Adv Mater Sci Eng. https://doi.org/10.1155/2014/273891
- Young, R. J. (2015). Composite micromechanics: From carbon fibres to graphene. In CS. P.W.R. Beaumont, A. Hodzic (Ed.), Woodhead Publishing Series in Composites Science and Engineering, Structural Integrity and Durability of Advanced Composites. Woodhead Publishing, Sawston, pp. 3–23. https://doi.org/10.1016/B978-0-08-100137-0.00001-8
- Zampaloni M, Pourboghrat F, Yankovich SA, Rodgers BN, Moore J, Drzal LT, Mohanty AK, Misra M (2007) Kenaf natural fiber reinforced polypropylene composites: a discussion on manufacturing problems and solutions. Compos A Appl Sci Manuf



38(6):1569–1580. https://doi.org/10.1016/j.compositesa.2007. 01.001

Zavan B, Gardin C, Guarino V, Rocca T, Maya IC, Zanotti F, Ferroni L, Brunello G, Chachques JC, Ambrosio L, Gasbarro V (2021) Electrospun pcl-based vascular grafts: In vitro tests. Nanomaterials 11(3):1–16. https://doi.org/10.3390/nano11030751

Zhong W, Li F, Zhang Z, Song L, Li Z (2001) Short fiber reinforced composites for fused deposition modeling. Mater Sci Eng, A 301(2):125–130. https://doi.org/10.1016/S0921-5093(00)01810-4

**Publisher's Note** Springer Nature remains neutral with regard to jurisdictional claims in published maps and institutional affiliations.

Springer Nature or its licensor (e.g. a society or other partner) holds exclusive rights to this article under a publishing agreement with the author(s) or other rightsholder(s); author self-archiving of the accepted manuscript version of this article is solely governed by the terms of such publishing agreement and applicable law.

